

Electrodynamic friction of a charged particle passing a conducting plate

Kimball A. Milton,^{1,*} Yang Li,^{1,†} Xin Guo,^{1,‡} and Gerard Kennedy^{2,§}

¹*H. L. Dodge Department of Physics and Astronomy,
University of Oklahoma, Norman, OK 73019, USA*

²*School of Mathematical Sciences, University of Southampton, Southampton, SO17 1BJ, UK*

(Dated: November 18, 2019)

The classical electromagnetic friction of a charged particle moving with prescribed constant velocity parallel to a planar imperfectly conducting surface is reinvestigated. As a concrete example, the Drude model is used to describe the conductor. The transverse electric and transverse magnetic contributions have very different character both in the low velocity (nonrelativistic) and high velocity (ultrarelativistic) regimes. Both numerical and analytical results are given. We also show how Vavilov-Čerenkov radiation can be treated in the same formalism.

I. INTRODUCTION

Over the past several decades there has been continuing theoretical interest in Casimir or quantum friction between dielectric bodies in relative motion, or between polarizable atoms and dielectric or conducting surfaces, but there has been no experimental confirmation of such effects. For a brief review with many references see Ref. [1]. In the course of our continuing investigations, we have also examined classically analogous effects. For example, a charged particle moving close to an imperfectly conducting surface experiences a drag force parallel to its motion. This was apparently first considered by Boyer [2], and revisited later [3–5]. Ohmic heating is the relevant physical mechanism [6], and the effects may have been observed in experiments with solid nitrogen sliding above (superconducting) lead [7–9], although, in such a case, quantum effects are likely to be more relevant [10].

Here we will extend these nonrelativistic studies into the relativistic regime, continuing to model the conductor by a Drude-type dispersion relation, and analyze the very different behaviors of the transverse electric (TE) and transverse magnetic (TM) contributions. The physical origin of the friction in the classical and quantum regimes is the same—the dissipation in the surface—so understanding this better in the classical case may yield useful insight into the quantum regime.

Of course, it will be recognised that, for real metals, the Drude model is only appropriate for $\omega \lesssim 1$ eV [11]. So, our work should be regarded mainly as an illustrative theoretical exercise. However, since the same methods can be generalized in a straightforward manner to a more appropriate description of an imperfect conductor, we would expect our results and conclusions to remain qualitatively correct in that context.

The outline of this paper is as follows. In Sec. II we set up our general formulation in terms of TE and TM Green's functions. The TE contribution is discussed in Sec. III, with analytic results for both low and high velocities, while a similar treatment for the somewhat more complex, but more important, TM contribution is given in Sec. IV. A brief discussion of possibilities of observing such effects is given in Sec. V. Appendix A gives a bit more detail about the electromagnetic Green's functions, while Appendix B shows how analytic expressions for integrals encountered in the high-velocity limit are obtained. Appendix C shows how the same formulation can be used to describe the motion of a particle in a uniform dielectric medium, and the force on the charged particle due to Vavilov-Čerenkov radiation is rederived.

In this paper we will use Heaviside-Lorentz units with $c = 1$.

II. GENERAL EXPRESSIONS

The idea is very simple. A particle of charge e is moving with velocity \mathbf{v} parallel to a plane conducting surface. It experiences a Lorentz force

$$\mathbf{F} = e(\mathbf{E} + \mathbf{v} \times \mathbf{B}). \quad (2.1)$$

* kmilton@ou.edu

† liyang@ou.edu

‡ guoxinmike@ou.edu

§ g.kennedy@soton.ac.uk

Here, the electric field arises because of the image charge induced by the conducting plane. The field may be expressed in terms of a suitable Green's dyadic. This may be most conveniently written in the frequency domain:

$$\mathbf{E}(\mathbf{r}; \omega) = -\frac{1}{i\omega} \int (d\mathbf{r}') \mathbf{\Gamma}(\mathbf{r}, \mathbf{r}'; \omega) \cdot \mathbf{j}(\mathbf{r}'; \omega). \quad (2.2)$$

(For the connection with the perhaps more familiar Green's function expressed in terms of vector potentials, see the Appendix of Ref. [12]. For further details, see Appendix A.) The magnetic field does no work on the particle, so may be disregarded. Here the current is that due to the particle moving with prescribed constant velocity $\mathbf{v} = v\hat{\mathbf{x}}$, where the particle is a distance a in the z direction above the surface of the conductor:

$$\mathbf{j}(\mathbf{r}, t) = ev\delta(\mathbf{r} - a\hat{\mathbf{z}} - \mathbf{v}t) = ev\hat{\mathbf{x}}\delta(x - vt)\delta(y)\delta(z - a). \quad (2.3)$$

We choose this representation for the Green's dyadic because it is precisely the retarded version of that used in the quantum calculations that are our main focus. Because the conductor lies in the x - y plane, we have translational invariance in that plane, which permits a transverse Fourier transform,

$$\mathbf{\Gamma}(\mathbf{r}, \mathbf{r}'; \omega) = \int \frac{(d\mathbf{k}_\perp)}{(2\pi)^2} e^{i\mathbf{k}_\perp \cdot (\mathbf{r} - \mathbf{r}')_\perp} \mathbf{g}(z, z'; \mathbf{k}_\perp, \omega), \quad k^2 = \mathbf{k}_\perp^2. \quad (2.4)$$

Inserting this construction into the Lorentz force formula, we immediately obtain the frictional force along the direction of motion,

$$F = F_x = -\frac{e^2}{2\pi i} \int_{-\infty}^{\infty} \frac{d\omega}{\omega} \int_{-\infty}^{\infty} \frac{dk_y}{2\pi} g_{xx}(a, a; k_x = \omega/v, k_y, \omega), \quad (2.5)$$

because the integration over x' provides a δ function in $k_x - \omega/v$. The Green's function appearing here can be written in terms of TE and TM parts, denoted by E and H superscripts, respectively, in an arbitrary background dielectric medium described by $\varepsilon(z; \omega)$:

$$g_{xx}(z, z'; k_x, k_y, \omega) = \frac{k_y^2}{k^2} \omega^2 g^E(z, z'; \kappa, \omega) + \frac{k_x^2}{k^2} \frac{1}{\varepsilon(z; \omega)} \frac{1}{\varepsilon(z'; \omega)} \partial_z \partial_{z'} g^H(z, z'; \kappa, \omega). \quad (2.6)$$

Here $\kappa = \sqrt{k^2 - \omega^2}$, and in the vacuum region $z > 0$ above the conductor

$$g^{E,H}(z, z'; \kappa, \omega) = \frac{1}{2\kappa} \left(e^{-\kappa|z-z'|} + r^{E,H} e^{-\kappa(z+z')} \right). \quad (2.7)$$

Here the reflection coefficients at the interface of the uniform conductor with the vacuum are

$$r^E = \frac{\kappa - \kappa'}{\kappa + \kappa'}, \quad r^H = \frac{\kappa - \kappa'/\varepsilon}{\kappa + \kappa'/\varepsilon}, \quad (2.8)$$

in terms of $\kappa' = \sqrt{\kappa^2 - \omega^2(\varepsilon(\omega) - 1)}$.

The $1/i$ appearing in the frictional force (2.5) is an instruction to take the imaginary part. (Actually, the real part integrates to zero.) One might suppose that the propagation constant κ would be complex, but due to the fact that $k_x = \omega/v$, that is entirely positive,

$$\kappa^2 = \frac{\omega^2}{\gamma^2 - 1} + k_y^2. \quad (2.9)$$

Hence, only the parts of the Green's functions that are proportional to the reflection coefficients can contribute. Here we have introduced the usual relativistic dilation factor, $\gamma = (1 - v^2)^{-1/2}$. Then the frictional force can be written in the following general form

$$F = -\frac{e^2}{8\pi^2} (\gamma^2 - 1) \int_0^\infty d\kappa \kappa e^{-2\kappa a} \int_0^{2\pi} d\theta \frac{\cos \theta}{(\gamma^2 - 1) \cos^2 \theta + 1} [f^E(\gamma, \kappa, \theta) + f^H(\gamma, \kappa, \theta)], \quad (2.10)$$

where

$$f^E(\gamma, \kappa, \theta) = 2 \sin^2 \theta \Im \left[1 + \sqrt{1 - (\gamma^2 - 1)(\varepsilon - 1) \cos^2 \theta} \right]^{-1}, \quad (2.11a)$$

$$f^H(\gamma, \kappa, \theta) = 2 \frac{\gamma^2}{\gamma^2 - 1} \Im \left[1 + \frac{1}{\varepsilon} \sqrt{1 - (\gamma^2 - 1)(\varepsilon - 1) \cos^2 \theta} \right]^{-1}. \quad (2.11b)$$

Here we have found it convenient to introduce polar coordinates by defining the two-dimensional vector

$$\boldsymbol{\kappa} = \left(\frac{\omega}{\sqrt{\gamma^2 - 1}}, k_y \right), \quad \kappa^2 = \kappa^2, \quad (2.12a)$$

so

$$\omega = \sqrt{\gamma^2 - 1} \kappa \cos \theta, \quad k_y = \kappa \sin \theta. \quad (2.12b)$$

In the following, in order to have a definite model, we adopt the damped plasma model (“Drude model”) for the permittivity:

$$\varepsilon(\omega) = 1 - \frac{\omega_p^2}{\omega^2 + i\nu\omega}, \quad (2.13)$$

where ω_p is the plasma frequency and ν is the damping parameter, assumed constant. In terms of our polar variables, this translates to

$$\varepsilon - 1 = - \frac{\omega_p^2}{(\gamma^2 - 1)\kappa^2 \cos^2 \theta + i\nu\kappa\sqrt{\gamma^2 - 1} \cos \theta}. \quad (2.14)$$

When we make specific numerical calculations, we can use approximate values for gold¹ [13]:

$$\hbar\omega_p = 9.0 \text{ eV}, \quad \hbar\nu = 0.035 \text{ eV}. \quad (2.15)$$

(Again, for comparison with the quantum case, it is convenient to use the quantum-mechanical energy conversion. The conversion factor $\hbar c = 2 \times 10^{-5} \text{ eV cm}$ is useful.)

Let us adopt dimensionless variables

$$u = 2\kappa a, \quad \alpha = 2\omega_p a, \quad \beta = 2\nu a, \quad (2.16)$$

and then write the force as

$$F = - \frac{e^2}{32\pi^2 a^2} \mathcal{F}, \quad (2.17)$$

wheres

$$\mathcal{F} = (\gamma^2 - 1) \int_0^\infty du u e^{-u} \int_0^{2\pi} \frac{d\theta \cos \theta}{(\gamma^2 - 1) \cos^2 \theta + 1} [f^E(u, \theta; \gamma; \alpha, \beta) + f^H(u, \theta; \gamma; \alpha, \beta)]. \quad (2.18)$$

III. TE CONTRIBUTION

Although it will turn out that the TE contribution is negligible compared to the TM part, it is easier to analyze, so we start with that. In the Drude model, the function f^E is

$$f^E(u, \theta; \gamma; \alpha, \beta) = 2 \sin^2 \theta \Im \left[1 + \sqrt{1 + \frac{\alpha^2}{u^2} \left(1 + i \frac{\beta}{u\sqrt{\gamma^2 - 1} \cos \theta} \right)^{-1}} \right]^{-1}. \quad (3.1)$$

The nonrelativistic limit, $\gamma \rightarrow 1$, is immediate:

$$f^E(u, \theta; \gamma; \alpha, \beta) \rightarrow \frac{\alpha^2}{4u\beta} (\gamma^2 - 1)^{1/2} \cos \theta \sin^2 \theta, \quad (3.2)$$

¹ More recent measurements by Olmon et al. [11] give roughly consistent values: $\hbar\omega_p = 8.5 \pm 0.5 \text{ eV}$ and $\hbar\nu = 0.050 \pm 0.011 \text{ eV}$. We continue to use our nominal values for illustrative purposes.

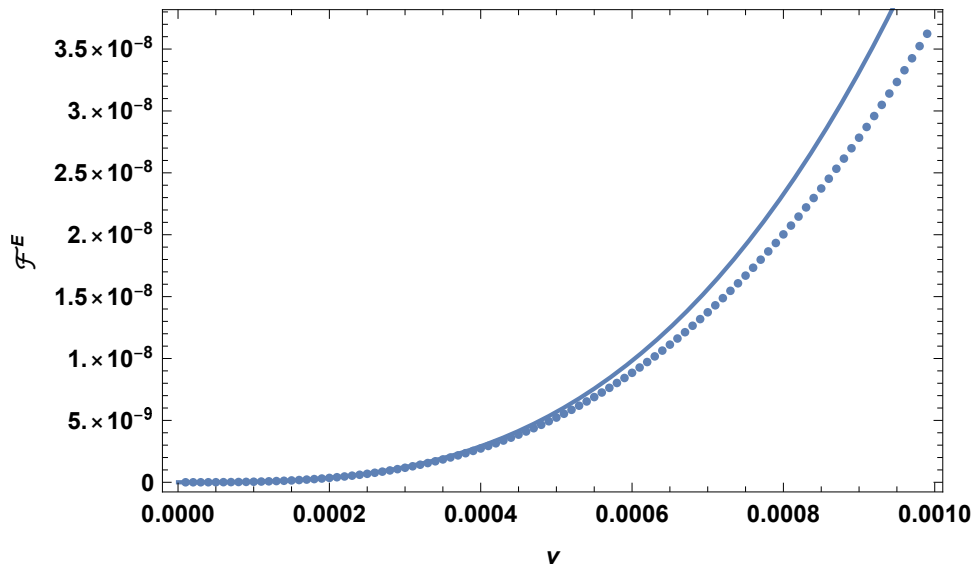


FIG. 1. The low velocity approximation to the TE friction (3.3) [solid curve] compared with the exact numerical integration the TE friction force in Eq. (2.18) [dotted curve]. Here we have chosen the separation distance of the particle from the plate to be $a = 10$ nm so for gold, $\alpha = 0.9$, $\beta = 0.0035$.

which, when inserted into Eq. (2.18), yields

$$\mathcal{F}^E = (\gamma^2 - 1)^{3/2} \frac{\pi}{16} \frac{\alpha^2}{\beta} = \frac{\pi}{16} \frac{v^3 \alpha^2}{\beta}, \quad v \ll \beta. \quad (3.3)$$

This agrees closely with the result of the direct numerical integration of the force for small velocity of the charged particle, as seen in Fig. 1.

Extracting the high-velocity limit is rather more subtle. Evidently, the friction vanishes if the damping is zero, $\beta = 0$, so it would seem to make sense to expand in powers of β . This is readily seen to yield

$$f^E(u, \theta; \gamma; \alpha, \beta) \approx \frac{\beta}{\sqrt{\gamma^2 - 1} \cos \theta} \frac{\alpha^2 \sin^2 \theta}{[u + \sqrt{u^2 + \alpha^2}]^2} \frac{1}{\sqrt{u^2 + \alpha^2}}. \quad (3.4)$$

For large γ , the θ integral is

$$\int_0^{2\pi} d\theta \frac{\sin^2 \theta}{\cos^2 \theta + \frac{1}{\gamma^2 - 1}} \approx 2\pi\gamma, \quad (3.5)$$

and the remaining u integral is

$$I_E(\alpha) = \int_0^\infty du u e^{-u} \frac{1}{\sqrt{u^2 + \alpha^2} (u + \sqrt{u^2 + \alpha^2})^2}, \quad (3.6)$$

which can be written in terms of Struve and Bessel functions [14]:

$$I_E(\alpha) = -\frac{4}{\alpha^4} + \frac{1}{3\alpha} - \frac{\pi}{2\alpha} [\mathbf{H}_1(\alpha) - Y_1(\alpha)] + \frac{\pi}{\alpha^2} [\mathbf{H}_2(\alpha) - Y_2(\alpha)]. \quad (3.7)$$

See Appendix B for more detail. In terms of this function, the TE friction in the $\gamma \rightarrow \infty$ limit approaches

$$\mathcal{F}^E \sim 2\pi\beta\alpha^2 I_E(\alpha) = 0.6533\beta \rightarrow 0.002287, \quad (3.8)$$

where the first number is for the $a = 10$ nm value of α for gold, $\alpha = 0.9$, and the second for the damping parameter $\beta = 0.0035$. In Fig. 2 we show that this linear behavior matches the exact integration quite well for low β . We explore the α dependence given in Eq. (3.8) in Fig. 3. Note, as further shown in Appendix B, that the force tends to zero as $\omega_p \rightarrow \infty$, as we might expect for a perfect conductor.

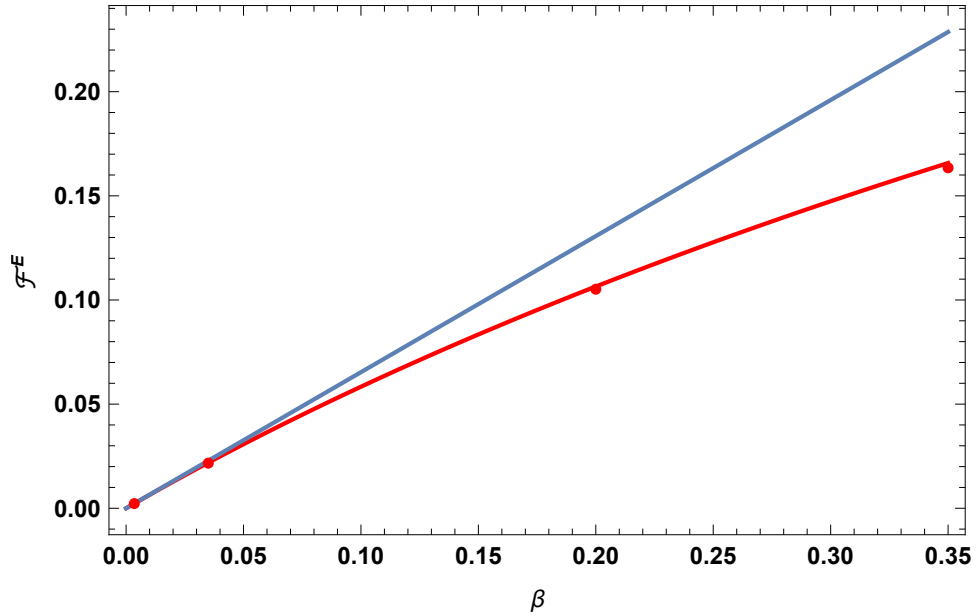


FIG. 2. The linear behavior (3.8) in the damping parameter β of the ultrarelativistic TE friction (upper blue line), compared with exact data (dots) for $\alpha = 0.9$, $\gamma = 100$. For larger values of β the data falls below the linear curve. The curve that matches the data well (red) is based on the more exact treatment (3.9).

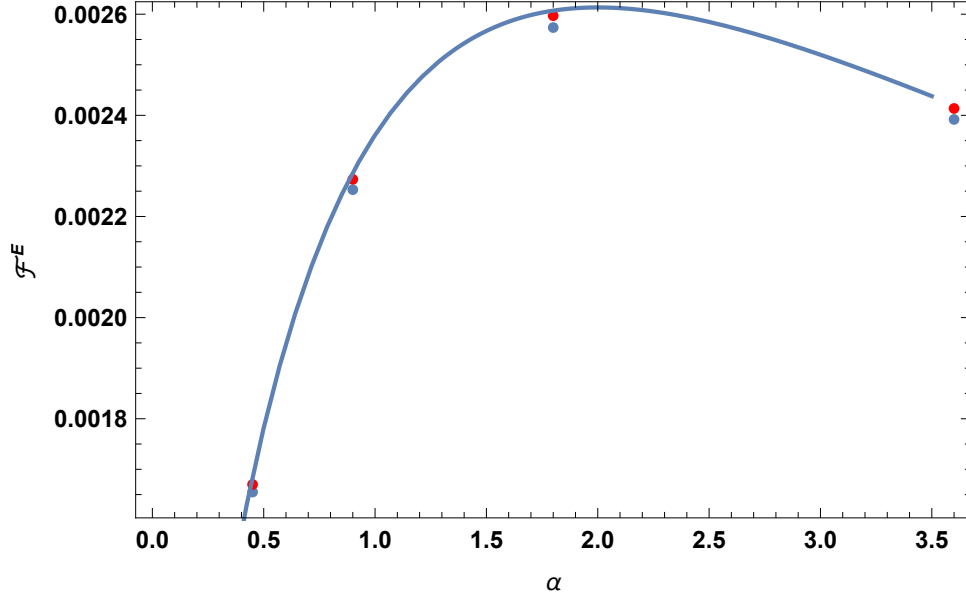


FIG. 3. The high-velocity TE frictional force given by Eq. (3.8) as a function of the dimensionless plasma frequency α for $\beta = 0.0035$ (solid curve). It is compared with numerical data from (2.18) for $\gamma = 1000$ (upper, red dots), and for $\gamma = 100$ (lower, blue dots). Agreement seems excellent, particularly for the larger value of γ .

The astute reader might question the validity of the expansion (3.4) in powers of the damping parameter β , since $\cos \theta = 0$ is included in the region of integration. So we can test this procedure, by breaking up the θ integration into two regions, $0 < \theta < \theta_0$, $\theta_0 < \theta < \pi/2$, where $\pi/2 - \theta_0 \ll 1$, but $\gamma \cos \theta_0 \gg 1$. Then the former region is easily seen to give a contribution to the friction which goes like $1/\gamma$ as $\gamma \rightarrow \infty$, while the latter can be approximately written as

$$\mathcal{F}^E \approx 8 \int_0^\infty du u e^{-u} \int_0^\infty d\phi \frac{\phi}{\phi^2 + 1} \Im \left(1 + \sqrt{1 + \frac{\alpha^2/u^2}{1 + i\beta/(u\phi)}} \right)^{-1}. \quad (3.9)$$

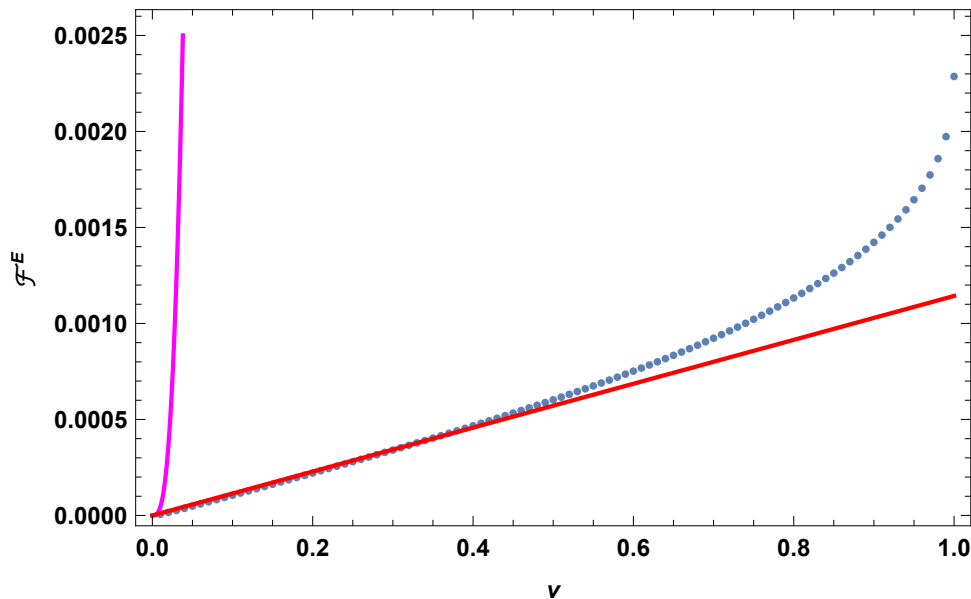


FIG. 4. The TE contribution to the friction for the whole range of charged particle velocities, for $\alpha = 0.9$, $\beta = 0.0035$. Shown also are the low-velocity (magenta curve) and high-velocity (final dot) limits. Note that the cubic behavior predicted for very low velocities cannot be seen on the scale of this graph. Instead, a linear behavior soon takes over for modest v . This is described by Eq. (3.10), shown by the red line.

Here $\phi = \gamma(\pi/2 - \theta)$. The result of the numerical integration of this is also shown in Fig. 2, which matches the linear behavior for small β , and the exact data for larger values of the damping. In particular, for our nominal values $\alpha = 0.9$, $\beta = 0.0035$, $\mathcal{F}^E = 0.002276$.

We conclude this section by showing the behavior of \mathcal{F}^E for all v in Fig. 4. The predominant linear region seen in Fig. 4 is easily reproduced by using the small β expansion in Eq. (3.4), but now letting γ approach 1:

$$\mathcal{F}^E \approx \pi\beta v\alpha^2 I_E(\alpha), \quad v \ll 1, \quad (3.10)$$

approaching half the value in Eq. (3.8) as $v \rightarrow 1$. The agreement with numerical integration is good.

IV. TM CONTRIBUTION

We turn now to the dominant TM contribution, which is, in general, rather more subtle. The $v \rightarrow 0$ limit is easy, since the leading contribution in the low v limit is

$$f^H(v, \omega) \rightarrow \frac{4\omega a}{v^2} \frac{\beta}{\alpha^2}. \quad (4.1)$$

Inserting this into the formula for the force (2.10) we find the low-velocity limit as given by Ref. [2]:

$$F^H \sim -\frac{e^2}{8\pi a^2} \frac{\beta v}{\alpha^2} = -\frac{e^2}{16\pi} \frac{\nu v}{\omega_p^2 a^3}, \quad v \ll \beta, \quad (4.2)$$

noting that the connection between the Drude-model parameters and the Ohmic conductivity at zero frequency is $\sigma(0) = \omega_p^2/\nu$. This is much larger than the F^E contribution given in Eq. (3.3). We demonstrate that this agrees with the exact numerical integration of the TM force in Fig. 5.

Turning to the high velocity limit, we note that the expansion method in β that worked well in the TE case fails. This is because the force in this case is no longer analytic in β ; the integrand in the friction develops a singularity at $\beta = 0$. So instead we proceed by a numerical method, that described in the penultimate paragraph of Sec. III. The large γ behavior is captured by the integration over a small region of θ , $\theta_0 < \theta < \pi/2$, and is given in the limit of large γ by

$$\mathcal{F}^H \sim 8 \int_0^\infty du u e^{-u} \int_0^\infty d\phi \frac{\phi}{\phi^2 + 1} \Im \left\{ 1 + \left[1 - \frac{\alpha^2}{u^2 \phi^2 (1 + i\beta/(u\phi))} \right]^{-1} \sqrt{1 + \frac{\alpha^2/u^2}{1 + i\beta/(u\phi)}} \right\}^{-1}. \quad (4.3)$$

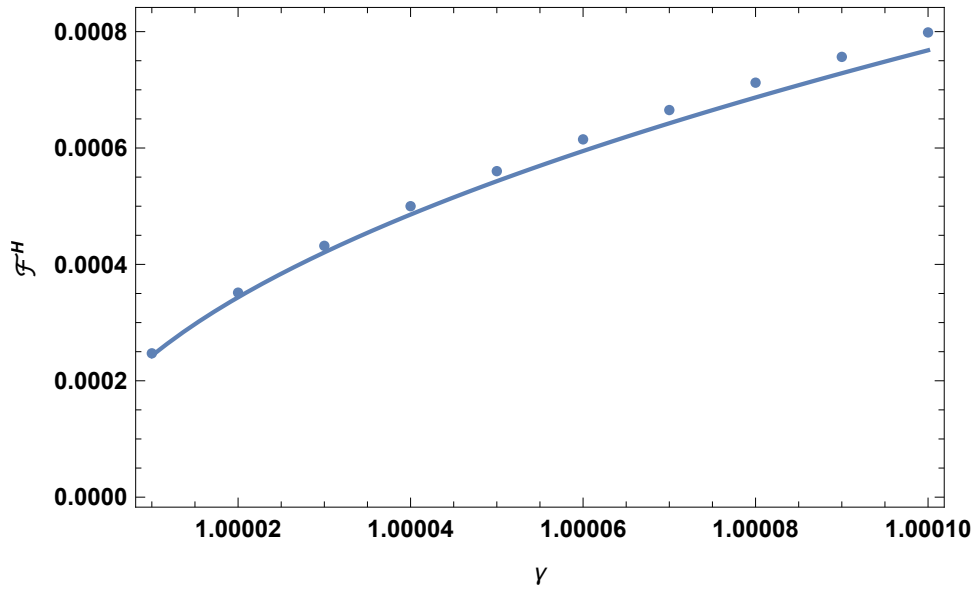


FIG. 5. The low velocity expression for the TM frictional force (written in terms of γ , solid curve) compared with the exact numerical integration (dots). Again the parameters are $\alpha = 0.9$ and $\beta = 0.0035$. Agreement is very good for small velocities.

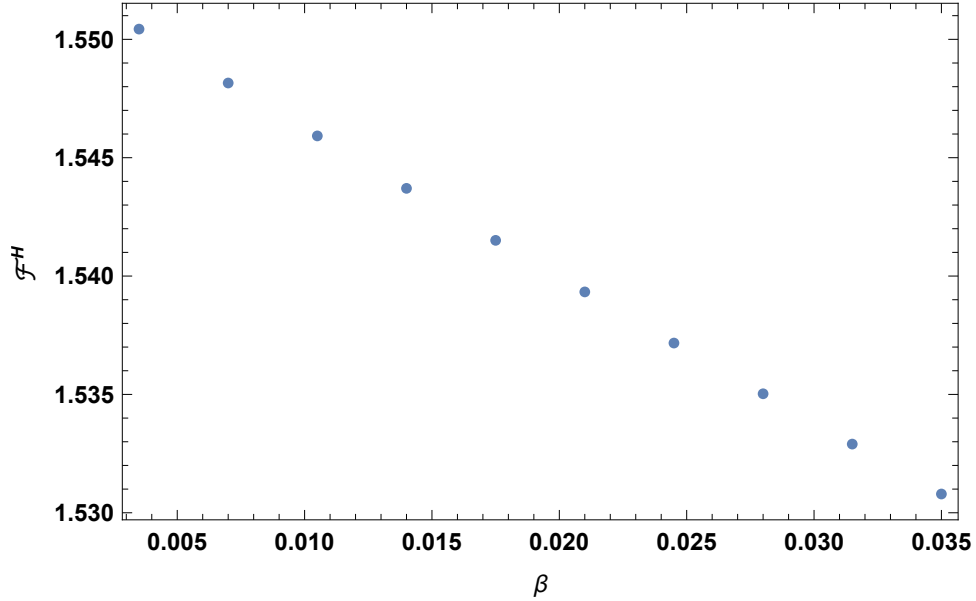


FIG. 6. The TM frictional force in the $\gamma \rightarrow \infty$ limit for $\alpha = 0.9$ and $\beta = 0.0035$. Note there is a mild linear dependence on the damping parameter β , and that the force tends to a nonzero value for $\beta \rightarrow 0+$.

This is plotted in Fig. 6. It is seen that the TM frictional force has a weak linear behavior in β , but tends to a nonzero value as $\beta \rightarrow 0$ through positive values. The latter can be extracted by considering the pole that develops in the integrand at $\beta = 0$, and approximating that structure by

$$\Im \frac{1}{\lambda(\phi^2 - \phi_0^2) + i\epsilon} = -\pi\delta(\lambda(\phi^2 - \phi_0^2)), \quad \lambda = u + \sqrt{u^2 + \alpha^2}, \quad \phi_0^2 = \frac{\alpha^2}{\lambda u}. \quad (4.4)$$

In this way we readily obtain the limiting value ($\gamma \rightarrow \infty$, $\beta \rightarrow 0$)

$$\mathcal{F}^H \rightarrow 4\pi\alpha^2 I_H(\alpha) = \frac{4\pi}{\alpha^2} \int_0^\infty du u e^{-u} \left(u - \sqrt{u^2 + \alpha^2}\right)^2 = 1.553, \quad \alpha = 0.9. \quad (4.5)$$

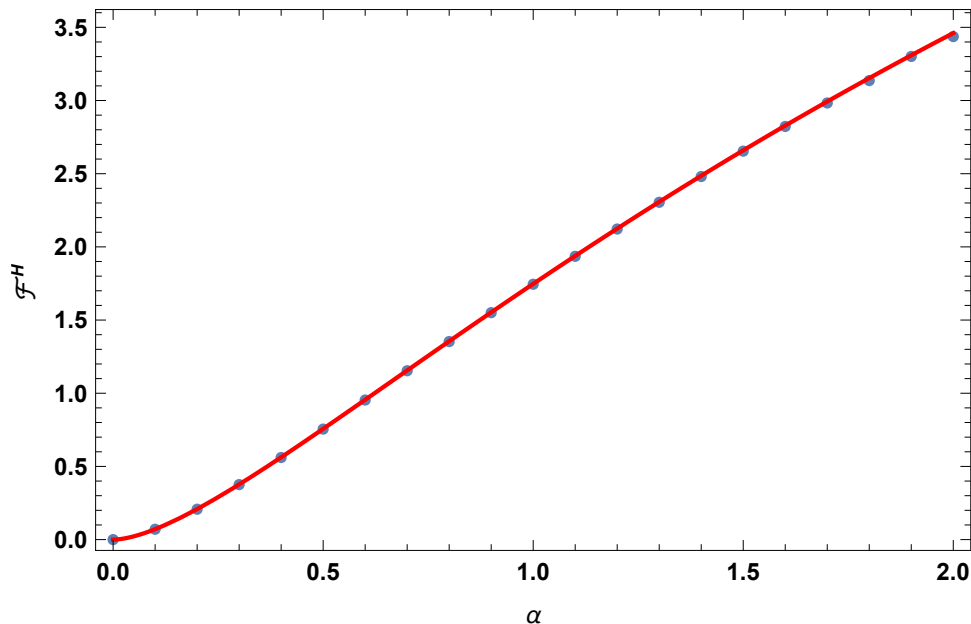


FIG. 7. Dependence of the high-velocity limit of the TM frictional force on the plasma frequency α . Here we have taken the damping parameter to be $\beta = 0.0035$. The dots come from the integration of Eq. (4.3), while the red curve is the function in Eq. (4.5).

(See Appendix B for an explicit form for this integral.) The dependence of the high-velocity limit as a function of the plasma frequency is shown in Fig. 7. Here we have taken the damping parameter to be $\beta = 0.0035$. The dots come from the integration of Eq. (4.3) while the curve comes from the limiting form (4.5). As shown in Appendix B, $\alpha^2 I_H(\alpha) \rightarrow 1$ as $\alpha \rightarrow \infty$. The difference between the dependencies of the frictional force on the plasma frequency shown in Figs. 7 and 3 is striking. The reason that the TM frictional force tends to a constant as $\omega_p \rightarrow \infty$, rather than zero as in the TE case, is due to the fact that here the dominant values of $2a\omega$ are of order $\sqrt{\alpha}$, not of order one. Thus, no perfect conductor limit is obtainable in this situation.

Finally, we show the TM frictional force for the whole range of velocities in Fig. 8. The difference with the TE force seen in Fig. 4 is remarkable. Not only is the value of the TE force three orders of magnitude smaller, but the TM force is nonmonotonic in the velocity. It is surprising that the maximum of the frictional force occurs for an intermediate value of the velocity.

V. CONCLUSIONS

In this paper we have reconsidered classical friction between a charged particle and an imperfectly conducting plate. We describe the latter by the Drude model. Only the nonrelativistic regime had been considered previously, to our knowledge. We examine both the TE mode, which is quite negligible in practice, and the TM mode. The low velocity limit is very straightforward to analyze, but the limit of high velocities (ultrarelativistic) is considerably more subtle. We obtain results for all velocities by a combination of analytic and numerical techniques.

How big are these effects, and might they be experimentally measurable? We compare the largest value of the TM friction, $\mathcal{F}^H \approx 3.5$, from Fig. 8, with the force on a static charged particle next to a conducting plate, $F_c = -e^2/(2a)^2$. The ratio is maximum at about 0.4 times the speed of light:

$$\frac{F}{F_c} \leq 0.044. \quad (5.1)$$

This is not large, but should be readily observable. This ratio drops to about 2% for an ultrarelativistic charged particle.

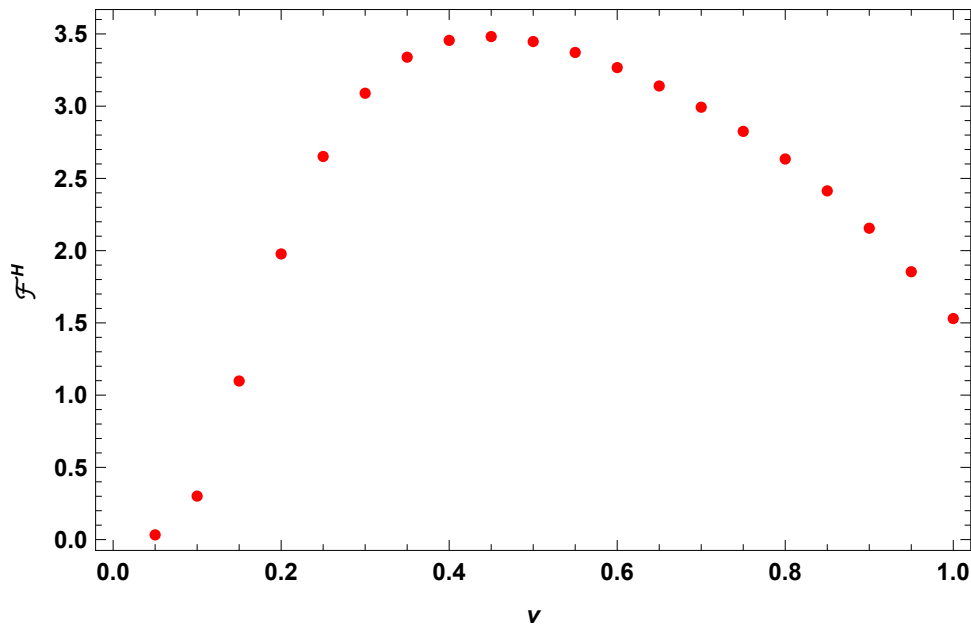


FIG. 8. The TM frictional force for all v , computed from the general formula (2.18). Because that formula is rather unstable for small β , we show the results for $\beta = 0.035$, ten times our nominal value, but in fact the results are nearly independent of β . Note that the linear region for very small v seen in Fig. 5 cannot be discerned on this graph.

ACKNOWLEDGMENTS

We thank our collaborators, Prachi Parashar, Steve Fulling, Hannah Day, and Aaron Swanson, for many helpful comments. This work was supported in part by a grant from the US National Science Foundation, grant number 1707511.

Appendix A: Electromagnetic Green's Function

Maxwell's equations in a medium characterized by position- and frequency-dependent permittivity ε and permeability μ yield the wave equation for the electric field

$$\nabla \times \frac{1}{\mu} \nabla \times \mathbf{E} - \omega^2 \varepsilon \mathbf{E} = i\omega \mathbf{j}, \quad (\text{A1})$$

where $\mathbf{E} = \mathbf{E}(\mathbf{r}; \omega)$, $\mathbf{j} = \mathbf{j}(\mathbf{r}; \omega)$. The electromagnetic Green's dyadic satisfies a similar equation,

$$\left[\frac{1}{\omega^2} \nabla \times \frac{1}{\mu} \nabla \times - \varepsilon \right] \mathbf{\Gamma}(\mathbf{r}, \mathbf{r}'; \omega) = \mathbf{1} \delta(\mathbf{r} - \mathbf{r}'). \quad (\text{A2})$$

From this Eq. (2.2) immediately follows. For the decomposition into TE and TM components, see Refs. [12, 15]

Appendix B: Evaluation of Integrals

It is straightforward to show that the integrals occurring in the ultrarelativistic ($v \rightarrow 1$) limit for \mathcal{F}^H

$$I_H(\alpha) = \int_0^\infty du e^{-u} \frac{u}{(u + \sqrt{u^2 + \alpha^2})^2} \quad (\text{B1})$$

and in the ultrarelativistic limit for \mathcal{F}^E

$$I_E(\alpha) = \int_0^\infty du e^{-u} \frac{u}{\sqrt{u^2 + \alpha^2} (u + \sqrt{u^2 + \alpha^2})^2} \quad (\text{B2})$$

may be expressed in terms of Struve and Bessel functions² by using [14]

$$\int_0^\infty du e^{-u} (u^2 + \alpha^2)^{\nu-1} = \frac{\sqrt{\pi}}{2} (2\alpha)^{\nu-\frac{1}{2}} \Gamma(\nu) \left[\mathbf{H}_{\nu-\frac{1}{2}}(\alpha) - Y_{\nu-\frac{1}{2}}(\alpha) \right]. \quad (\text{B3})$$

Thus,

$$\begin{aligned} I_H(\alpha) &= \frac{1}{\alpha^4} \int_0^\infty du e^{-u} u \left(u - \sqrt{u^2 + \alpha^2} \right)^2 \\ &= \frac{1}{\alpha^4} \int_0^\infty du e^{-u} \left(\alpha^2 u + 2u^3 + 2\alpha^2 \sqrt{u^2 + \alpha^2} - 2(u^2 + \alpha^2)^{\frac{3}{2}} \right) \\ &= \frac{12}{\alpha^4} + \frac{1}{\alpha^2} + \frac{\pi}{\alpha} [\mathbf{H}_1(\alpha) - Y_1(\alpha)] - \frac{3\pi}{\alpha^2} [\mathbf{H}_2(\alpha) - Y_2(\alpha)]. \end{aligned} \quad (\text{B4})$$

Likewise,

$$\begin{aligned} I_E(\alpha) &= \frac{1}{\alpha^4} \int_0^\infty du e^{-u} \frac{u \left(u - \sqrt{u^2 + \alpha^2} \right)^2}{\sqrt{u^2 + \alpha^2}} \\ &= \frac{1}{\alpha^4} \int_0^\infty du e^{-u} \frac{(-\alpha^2 u + 2u(u^2 + \alpha^2) - 2u^2 \sqrt{u^2 + \alpha^2})}{\sqrt{u^2 + \alpha^2}} \\ &= \frac{1}{\alpha^4} \int_0^\infty du e^{-u} \left(-\alpha^2 \frac{d}{du} \sqrt{u^2 + \alpha^2} + \frac{2}{3} \frac{d}{du} (u^2 + \alpha^2)^{\frac{3}{2}} - 2u^2 \right) \\ &= \frac{1}{\alpha^4} \left[\frac{\alpha^3}{3} + \int_0^\infty du e^{-u} \left(-\alpha^2 \sqrt{u^2 + \alpha^2} + \frac{2}{3} (u^2 + \alpha^2)^{\frac{3}{2}} - 2u^2 \right) \right] \\ &= -\frac{4}{\alpha^4} + \frac{1}{3\alpha} - \frac{\pi}{2\alpha} [\mathbf{H}_1(\alpha) - Y_1(\alpha)] + \frac{\pi}{\alpha^2} [\mathbf{H}_2(\alpha) - Y_2(\alpha)]. \end{aligned} \quad (\text{B5})$$

For small values of α , standard expansions of $\mathbf{H}_n(\alpha)$ and $Y_n(\alpha)$ may be used to evaluate these functions:

$$\alpha^2 I_H \sim -\frac{\alpha^2}{16} \left(1 + 4\gamma_E + 4 \ln \frac{\alpha}{2} \right) + \frac{4}{15} \alpha^3 + \dots, \quad (\text{B6a})$$

$$\alpha^2 I_E \sim \frac{\alpha}{3} - \frac{\alpha^2}{16} \left(1 - 4\gamma_E - 4 \ln \frac{\alpha}{2} \right) - \frac{1}{5} \alpha^3 + \dots, \quad (\text{B6b})$$

in terms of Euler's constant, $\gamma_E = 0.57721\dots$. For large values of α , the following asymptotic expansion [14] may be employed:

$$\mathbf{H}_n(\alpha) - Y_n(\alpha) = \frac{1}{\pi} \sum_{m=0}^{p-1} \frac{\Gamma(m + \frac{1}{2})}{\Gamma(n + \frac{1}{2} - m)} \left(\frac{\alpha}{2} \right)^{n-1-2m} + O(\alpha^{n-1-2p}). \quad (\text{B7})$$

It follows that

$$\alpha^2 I_H \rightarrow 1 - \frac{4}{\alpha}, \quad \alpha^2 I_E \rightarrow \frac{1}{\alpha} - \frac{4}{\alpha^2}, \quad \text{as } \alpha \rightarrow \infty. \quad (\text{B8})$$

We illustrate the behavior of these functions in Fig. 9.

Appendix C: Vavilov-Čerenkov Radiation

To illustrate the further utility of our Green's function approach, we apply Eqs. (2.5) and (2.6) to the situation of a charged particle moving through a homogeneous nondissipative dielectric material faster than the speed of light in

² It is interesting to note that the general formulas given, for example in Ref. [5], for the nonrelativistic case involve the same combination of Struve and Bessel functions, in that case $\mathbf{H}_0(\xi) - Y_0(\xi)$, where $\xi = \pi\alpha^2/(\beta v)$. However, beyond the leading low-velocity term (4.2), the corrections they give are very small, and do not describe the deviation from linearity that we see, for example, in Fig. 5.

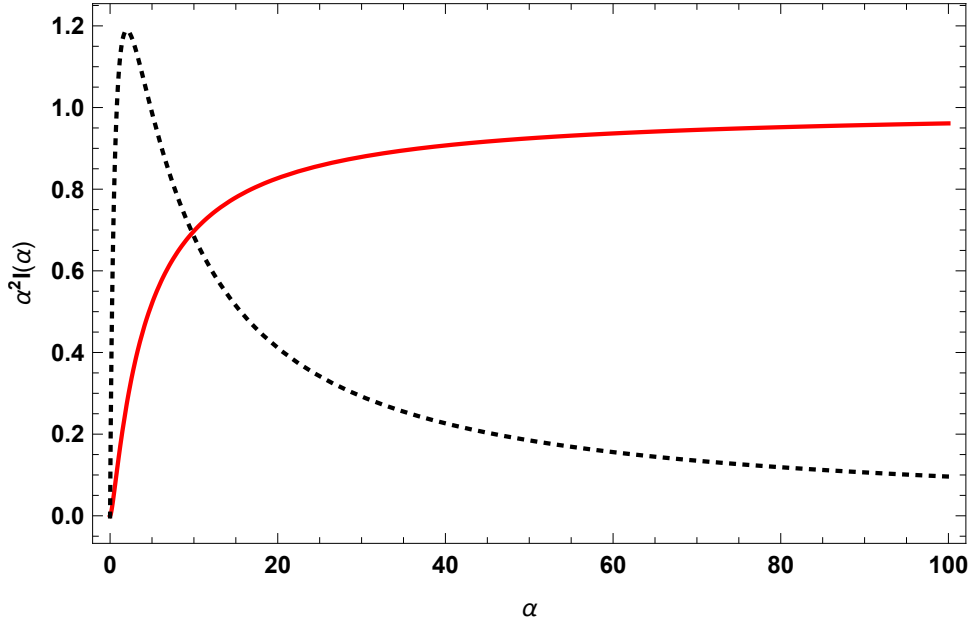


FIG. 9. Behavior of the integrals $\alpha^2 I_{H,E}$ as a function of the plasma frequency parameter α . The TE contribution (black, dotted) $\alpha^2 I_E$ is multiplied by a factor of 10, so the two functions may be shown on the same graph. The TM integral $\alpha^2 I_H$ is shown by the solid red curve. These functions describe the high-velocity limit of the frictional force, according to Eqs. (4.5) and (3.8).

the medium, $1/n = 1/\sqrt{\epsilon}$. In this case we will disregard dissipation in the material, setting $\nu = 0$; the imaginary part comes from the region of frequencies where $v > 1/n(\omega)$. The TE part of the drag on the particle is given by

$$F^E = -\frac{e^2}{2\pi} \int \frac{d\omega}{\omega} \int_{-\infty}^{\infty} \frac{dk_y}{2\pi} \frac{\omega^2}{k_y^2 + \omega^2/v^2} k_y^2 \Im \frac{1}{2\kappa'}, \quad (\text{C1})$$

since we now only have the bulk (first) term in Eq. (2.7), except that the particle is in the medium, so $1/(2\kappa) \rightarrow 1/(2\kappa')$. The branch line is chosen to run between the two branch points, where $k_y^2 = n(\omega)^2 \omega^2 [1 - 1/(n(\omega)^2 v^2)]$, on the real k_y axis. The subtlety is the sign of the imaginary part. This is resolved by noting that the retarded Green's function must have singularities only in the lower-half ω plane, which is consistent with the requirement that, in the case of infinitesimal damping, $n(\omega)^2 \omega^2$ has an imaginary part $\epsilon \text{sgn}(\omega)$, with $\epsilon \rightarrow 0+$. Therefore, the k_y integration passes below the branch line for $\omega > 0$, and above for $\omega < 0$. In dimensionless form, that integral then is

$$\int_{-1}^1 dx \frac{x^2}{x^2 + a^2} \frac{\text{sgn} \omega}{\sqrt{1-x^2}} = \pi \text{sgn}(\omega) \left(1 - \frac{a}{\sqrt{1+a^2}} \right), \quad (\text{C2})$$

with $a = \left(vn(\omega) \sqrt{1 - 1/(vn(\omega))^2} \right)^{-1}$, so that the above integral is simply $\text{sgn}(\omega) \pi [1 - 1/(vn(\omega))]$. The resulting drag force due to Čerenkov radiation is

$$F^E = -\frac{e^2}{8\pi} \int d\omega |\omega| \left(1 - \frac{1}{n(\omega)v} \right), \quad (\text{C3})$$

where the integral is over the region where $n(\omega) > 1/v$.

The TM contribution to the drag force is

$$F^H = \frac{e^2}{2\pi} \int \frac{d\omega}{\omega} \int_{-\infty}^{\infty} \frac{dk_y}{2\pi} \frac{\omega^2/v^2}{k_y^2 + \omega^2/v^2} \Im \left[\frac{\kappa'^2}{\epsilon(\omega)^2} \frac{\epsilon(\omega)}{2\kappa'} \right], \quad (\text{C4})$$

because except in the exponent, the TM Green's function is obtained from that for TE by the replacement $\kappa' \rightarrow \kappa'/\epsilon$. After doing the k_y integral as above, which now is

$$-\text{sgn}(\omega) \int_{-1}^1 dx \frac{\sqrt{1-x^2}}{x^2 + a^2} = \pi \text{sgn}(\omega) (1 - vn(\omega)), \quad (\text{C5})$$

we have

$$F^H = -\frac{e^2}{8\pi} \int d\omega |\omega| \frac{1}{n(\omega)v} \left(1 - \frac{1}{n(\omega)v}\right). \quad (\text{C6})$$

Adding the two modes together,

$$F = F^E + F^H = -\frac{e^2}{4\pi} \int d\omega \omega \left(1 - \frac{1}{n(\omega)^2 v^2}\right), \quad (\text{C7})$$

where now the integration is over *positive* frequencies for which the speed of the particle exceeds that of light in the medium, $1/n(\omega)$. This formula exactly coincides with the energy loss rate found in Eq. (36.19) of Ref. [15] due to the energy radiated by Vavilov-Čerenkov effect. (Note, Gaussian units were used there, and $e_{\text{HL}}^2 = 4\pi e_{\text{G}}^2$.)

- [1] K. A. Milton, J. S. Høye and I. Brevik, “The reality of Casimir friction,” *Symmetry* **8**, no. 5, 29 (2016) doi:10.3390/sym8050029 [arXiv:1508.00626 [quant-ph]].
- [2] T. H. Boyer, “Penetration of the electric and magnetic velocity fields of a nonrelativistic point charge into a conducting plane,” *Phys. Rev. A* **9**, 68–82 (1974).
- [3] T. H. Boyer, “Penetration of electromagnetic velocity fields through a conducting wall of finite thickness,” *Phys. Rev. E* **53**, 6450–6459 (1996).
- [4] M. S. Tomassone and A. Widom, “Electronic friction forces on molecules moving near metals,” *Phys. Rev. B* **56**, 4938–4943 (1997).
- [5] M. S. Tomassone and A. Widom, “Friction forces on charges moving outside a conductor due to Ohm’s law heating inside of a conductor,” *Am. J. Phys.* **65**, 1181–1183 (1997).
- [6] J. B. Sokoloff, “Kinetic friction due to Ohm’s law heating,” *J. Phys.: Condens. Matter* **14**, 5277–5287 (2002).
- [7] A. Dayo, W. Alnasrallah, and J. Krim, “Superconductivity-dependent sliding friction,” *Phys. Rev. Lett.* **80**, 1690–1693 (1998).
- [8] R. L. Renner, J. E. Rutledge, and P. Taborek, “Quantz microbalance studies of superconductivity-dependent sliding friction,” *Phys. Rev. Lett.* **83**, 1261 (1999).
- [9] J. Krim, “Krim replies,” *Phys. Rev. Lett.* **83**, 1262 (1999).
- [10] B. N. J. Persson, “Electronic friction on a superconducting surface,” *Solid State Comm.* **115**, 145–148 (2000).
- [11] R. L. Olmon, B. Slovik, T. W. Johnson, D. Shelton, S.-H. Oh, G. D. Boreman, and M. B. Raschke, “Optical dielectric function of gold,” *Phys. Rev. B* **86**, 235147 (2012).
- [12] J. Schwinger, L. L. DeRaad, Jr. and K. A. Milton, “Casimir effect in dielectrics,” *Ann. Phys. (N.Y.)* **115**, 1–23 (1979). doi:10.1016/0003-4916(78)90172-0
- [13] I. Brevik and J. B. Aarseth, “Temperature dependence of the Casimir effect,” *J. Phys. A* **39**, 6187–6193 (2006) [arXiv:quant-ph/0511037](Proc. 7th Workshop on Quantum Field Theory Under the Influence of External Conditions, Barcelona 5–9 September 2005, ed. E. Elizalde)
- [14] I. S. Gradshteyn, I. M. Ryzhik, Y. Y. Geronimus, M. Y. Tseytlin, A. Jeffrey, D. Zwillinger, V. H. Moll, (eds.), *Table of Integrals, Series, and Products*. Translated by Scripta Technica, Inc. (8 ed.). Academic Press, Inc. ISBN 978-0-12-384933-5.
- [15] J. Schwinger, L. L. DeRaad, Jr., K. A. Milton, and W.-y. Tsai, *Classical Electrodynamics* (Perseus, New York, 1998).